TARGETING THE MAIN PROTEASE AND THE SPIKE PROTEIN OF SARS-CoV-2 WITH NATURALLY OCCURRING COMPOUNDS FROM SOME CAMEROONIAN MEDICINAL PLANTS: AN IN-SILICO STUDY FOR DRUG DESIGNING

R. T. FOUEDJOU [a], H.P.D. FOGANG [b], M. OUASSAF [c], O. DAOUI [d], F. ABUL QAIS [e], S. ELKHATTABI [d], M. BAKHOUCH [f], S. BELAIDI [c] AND S. CHTITA [g]*

[a]*Research Unit of Environmental and Applied Chemistry, Department of Chemistry, Faculty of Science, University of Dschang, Box 67, Dschang, Cameroon.*
[b]*Department of Physiological Sciences and Biochemistry, Faculty of Medicine and Biomedical Sciences of Garoua, University of Ngaoundéré, Ngaoundéré, Cameroon.*
[c]*Group of Computational and Medicinal Chemistry, LMCE Laboratory, University of Biskra, Biskra, Algeria.*
[d]*Laboratory of Engineering, Systems and Applications, National School of Applied Sciences, Sidi Mohamed Ben Abdellah-Fez University, BP Box 72, Fez, Morocco.*
[e]*Department of Agricultural Microbiology, Faculty of Agricultural Sciences, Aligarh Muslim University, Aligarh-202002, India.*
[f]*Laboratory of Bioorganic Chemistry, Department of Chemistry, Faculty of Sciences, Chouaïb Doukkali University, P.O. Box 24, 24000 El Jadida, Morocco.*
[g]*Laboratory of Analytical and Molecular Chemistry, Faculty of Sciences Ben M'Sik, Hassan II University of Casablanca, B.P. 7955, Casablanca, Morocco*.

ABSTRACT

Despite the social distancing and hygiene rules prescribed by the WHO, the novel Corona-virus is still on the way of a significant rapid rise in deaths. Therefore, identification of chemotherapeutic drugs against Corona Viral Infection all around the world is still requires. Some medicinal plants have a valuable therapeutic effect when mixt with honey, the obtained formulations are preliminary use in Cameroon against viral infection particularly respiratory infections. In this work, we looked for the potential anti-SARS-CoV-2 molecule throw execution of *in silico* computational studies of six Cameroonian plants intervening in the treatment respiratory infections in apiphytotherapy. AutoDock Vina was used for docking studies against SARS-CoV-2 main protease (Mpro) and spike (SP) proteins. We further conducted of pharmacokinetics properties and the safety profile of compounds with the top score in order to identify the best drug candidates. Totally 100 compounds were screened, of these, eighteen showed high binding affinity against SARS-CoV-2 Mpro and SP. The results suggest the effectiveness of compounds **10** and **17** obtained from *Citrus Sinensis* as potent drugs against SARS-CoV-2 as they tightly bind to its Mpro and SP with low binding energies. The stability of the two compounds complexed with Mpro and SP was validated through MD simulation. The availability of potent protein inhibitors and diverse of compounds from Cameroon flora scaffolds indicate the feasibility of developing potent Mpro and SP proteins inhibitors as antivirals for COVID-19. Based on further *in vivo* and *in vitro* experiments and clinical trials, some of these phytoconstituents could be proposed for effective inhibition of the replication of the SARS-CoV-2.

Keywords: *COVID-19, SARS-CoV-2, Main protease, Spike protein, Apiphytotherapy, Molecular docking, Molecular dynamics, ADMET*.

1. INTRODUCTION

The month of November of 2019 turned out to be quite unexpected, with the advent of the coronavirus, which continues to influence our daily lives, and the challenges it has carried about creativity. Luckily, several vaccines have been developed and proposed for the urgent use against COVID-19. Among the proposed vaccines, few of them have been allowed to be used by the WHO [1]. However, several questions have been raised about the effectiveness, safety and the specificity of these vaccines. Several research team and pharmaceutical companies of different countries are diverting their best efforts for the implementation of appropriate preventive and control strategies. Most of them announced their headway and programs to develop vaccines (e.g. subunit, mRNA, DNA, live-vector vaccine) against this disease [2-4]. Neither vaccines nor direct-acting antiviral drugs are available for the treatment of human and animal coronavirus infections. So, the development of a new effective treatment is always needed to stop the propagation of the disease. There is an urgent need to develop a new effective treatment strategy for the proper and complete treatment of this disease. In addition, the exploration of the natural compounds using predictive studies appear as a promising path.

Literature survey reveals that there is a little scientific data available on plants used against respiratory diseases in Cameroon. Hence, it seems to be very interesting to explore its flora to promote medicinal plants in the treatment of these pathologies, in particular, Covid-19. Medicinal plants, especially those employed in the West region of Cameroon, have attracted significant attention. These plants are rich of bioactive compounds that could be used to develop drugs against several diseases with no or minimal side effects. The recipes made from Cameroonian medicinal plants against respiratory tract diseases have been characterized and the plants used in the preparation of these recipes have been identified. The secondary metabolites of some of these plants have been listed and their *in-silico* action on the SARS-CoV-2 was revealed in a previous study [5].

All over the world, interest in traditional medicine is growing steadily, especially in Africa, where the practice of this medicine requires considerable improvement [6]. In order to improve the effectiveness of the used recipes, they are very often used as juice or powder in combination with other natural products like honey. Beekeeping is well developed in the western highlands of Cameroon and honey is the most exploited product [7], [8]. The populations resort to self-medication based on medicinal plants combined with honey (apiphytotherapy) for relief. Apiphytotherapy is a form of traditional medicine, which combines medicinal plants, and bee products, particularly, honey. The ethnobotanical survey of 326 people on apiphytotherapy based on honey in the West Highlands of Cameroon has individualized 127 therapeutic recipes used for the treatment of approximately 113 diseases plaguing the area [9]. Therefore, natural therapies should inspire and complete the conquests of allopathic medicine and a symbiosis should be made between phytotherapy, apitherapy and chemotherapy considering the values and risks of each therapy method [10]. This work is part of a vast program of Cameroonian flora valorization following the Covid-19 pandemic, as has already been illustrated by recent work on some plants of the Asteraceae family [5].

The primary goal of this research is to identify phytochemical structures that are favorable for drug design for SARS-CoV-2 chemotherapy. The first point is to use of the results of ethnobotanical surveys obtained from traditional healers to identify the plants used in combinations with honey to treat respiratory tract ailments. Secondly, to identify based on literature survey, the compounds already isolated from these species in order to identify the active molecules and/or responsible for the treatment of respiratory diseases, in particular, SARS-CoV-2. Furthermore, we will combine molecular docking and dynamics simulations studies to propose lead compounds as potent inhibitors against SARS-CoV-2 Mpro (PDB ID: 6lu7) and SP proteins (PDB ID: 6moj).

2. MATERIALS AND METHODS

2.1. Molecular Docking

Molecular docking was performed to study the binding affinity and type of interactions between ligands from extensive literature search and the targets. The high-resolution X-ray structures of proteins with their defined active sites, and the top-predicted docking pose of each ligand with the highest binding score were

**Corresponding author email: samirchtita@gmail.com*

used as starting point for the molecular dynamic simulation. To prepare the ligands for docking, the structures of these compounds were drawn with the generation of their 3D structures using ChemSketch software and were retrieved and saved in PDB format, which were further saved in mol file followed by the subsequent optimization using Sybyl program.

2.2. Structural properties of selected target of SARS-CoV-2 and their preparation

To investigate some constituents of plants intervening in apiphytotherapy against the SARS-CoV-2 virus, we have selected two targets; the Mpro coded PDB ID: 6lu7 and the SP coded PDB ID: 6m0j. The active sites of the Mpro and the SP were determined and correspond to the coordinates: x= -10.641 Å, y = 11.847 Å, z= 68.346 Å and x= -34.933 Å, y = 8.672Å , z= 29.036 Å, respectively [5], [11]. They could allowed better define the potential target drug that may protect the world from the Covid-19 pandemic, which makes them key targets for therapeutics in SARS- CoV-2. The viral genome is encapsulated within a membrane envelope, where glycoprotein spike makes coronavirus appear crown-like. The crystal structure of the Mpro and the SP of SARS CoV-2 was downloaded in PDB format and protein preparation was carried out in Biovia Discovery Studio 2020 software (Dassault Systems BIOVIA, D.S.V., San Diego: Dassault Systems, 2020) [12].

2.2.1. Main protease (Mpro)

Mpro is known to help intracellular homeostasis in virus via various protein interactions. The entry of virus takes place in association with interaction of two Mpro, Mpro-SP, and Mpro-nucleocapsid protein. The introduction of SP in new virus takes place via M-S interactions. Mpro facilitates the generation and release of virus like particles. Hence, Mpro is known to potentiate sensitization of the cell host by virus [13]. This protease could be a validated target for developing antivirals as inhibitors of its activity, which will block maturation of viral proteins that are indispensable for viral replication.

2.2.2. Spike protein (SP)

Efforts to protect human cells against SARS-CoV-2 have focused on the trimeric SP. It is among the four structural proteins encoded by the viral RNA. Although the primary entry of the virus is mediated by ACE2 receptors forming complexes with SP, previous study via molecular docking demonstrated that there might be four regions in the SP that may act as binding sites [14]. It has been revealed that the SP of SARS-CoV-2 possess strong affinity for binding to human ACE-2 receptors [15] and it was found to have potential role in viral entry inside the host [16]. Therefore, SP is a potential target for drug discovery.

2.3. Phytochemicals dataset and ligand preparation

Decoctions of some plants are used in Cameroon in combination with honey to fight caught, angina, asthma, bronchitis, flu, pulmonary infections, laryngitis, pneumonia, cold, dry cough, …etc. [9]. A total of 100 bioactive constituents obtained from extensive literature research were selected to perform the molecular docking studies to screen and identify the potent antiviral agents for COVID-19. Left as it follows; 15, 16, 16, 3, 32 and 19 on *Zingiber officinale* (Zingiberaceae) [17-19], *Cymbopogon citratus* (Poaceae) [20-22], *Allium cepa* [23-27], *Allium sativum* L. (Alliaceae) [28], *Citrus sinensis* (Rutaceae) [29-31] and *Thymus vulgaris* [32-34] (Lamiaceae), respectively.

ChemSketch Software was used to prepare the PDB ligands structures. Ligands bioactive conformations was simulated and docked with the active binding site of the prepared protein. Interactions with amino acid residues were identified using Autodock Vina. The interactions of the docking result were obtained by importing our result to the Discovery Studio visualizer, hence, enabling us to identify significant interactions between the ligands and the protein and/or enzyme binding sites.

2.4. Prediction of the Pharmacokinetic Parameters

The purpose of pharmacokinetics is to study the fate of a drug in the body. Determining the pharmacokinetic parameters of a drug provides information that makes it possible to choose the routes of administration and to adapt the dosages for its future use. The four fundamental processes which influence the *in vivo* pharmacokinetics of a compound are absorption, distribution, metabolism and excretion (ADME) [36]. After molecular docking analysis in order to study the binding affinity and type of interactions, ligands that showed a strong binding affinity with 6lu7 and 6m0j proteins were selected for further investigations. This survey was undertaken to predict, filter and identify suitable lead candidates, using molecular dynamics simulation. ADME are imperative interest in the process of success of a drugs journey through the body and to prevent the failure of those compounds during clinical studies and enhance their chances to reach the stage of being drug candidates in the future. These parameters are investigated by pkCSM server (http://biosig.unimelb.edu.au/pkcsm/prediction) [37]. Toxicological purpose is the main considerations in case of the development of new drugs. The toxicity evaluation was carried out on the top potential hit compounds using the same online server.

2.5. Molecular dynamics simulations

Two hit compounds (compounds **10** and **17**) obtained through molecular docking were further explored thorough molecular dynamics (MD) simulation. The MD simulation was performed using amber99sb-ILDN force field with Gromacs-2018.1 packages [38], [39] following the same protocol as described in our previous studies [5]. The MD simulation of bot ligands was performed with two important proteins of SARS-CoV-2, *i.e.*, SARS-CoV-2 Mpro and spike receptor-binding domain. The topology of ligands was generated using AM1-BCC charge model with Antechamber packages in AmberTools19 [40]. The proteins and complexes were solvated separately in triclinic box using the TIP3P water model followed by the neutralization by adding counter (sodium or chlorine) ions. All systems were subjected to the steepest minimization of a maximum 5000 steps to remove the weak Van der Waals contacts. The systems were equilibrated for NVT at 300 K using V-rescale thermostat for 1 ns and then for NPT at 1.0 bar using Parrinello-Rahman barostat at 1.0 bar for 1 ns [41], [42]. The standard MD simulation was carried out until 100 ns for each system in which 10000 frames of each trajectory was stored at 10 ps intervals. Before analysis, all trajectories were subjected to PBC corrections. All analysis was performed using standard Gromacs utilities. For MM-PBSA calculations, 100 frames from the trajectory of each complex were extracted to calculate various binding energies [43].

3. RESULTS AND DISCUSSION

3.1. Phytochemical database

The current *in silico* study was undertaken to identify efficient antivirals compounds against Covid-19. For this purpose, a bibliographic survey conducted in the field of apiphytotherapy permit to enumerated six plants used in the west region of Cameroon as shown in the Table 1.

Table 1: Some used plants in apiphytotherapy against respiratory infections [8].

Combined plants with honey	Plant's part use	Pharmacological activity
Zingiber officinale Hook.	Roots	Flu, rheum, angina and bronchitis
Cymbopogon citratus (Dc.) Stapf	Whole plant Leaves	Angina, dry cough Pulmonary infections
Allium cepa L.	Fruit (Bulbe)	Pneumonia
Allium sativum L.	Gousse	angina, rhinitis, bad breath, Asthma, laryngitis, bronchitis
Citrus sinensis L.	Leaves, fruits	Rheum, bad breath, pneumonia, airway cleaning
Thymus vulgaris L.	Leaves, fruits	Airway cleaning

A literature data let us to identify nearly 250 compounds belonging to the above described plants. Approximate application of the 3rd Lipinski's rule relative to molecular weight [44], led to filter out non drug like molecules, which allowed us to narrow down the database to 100 compounds distributed as follow: *Z. officinale* (15), *C. citratus* (16), *A. cepa* (16), *A. sativum* L. (3), *C. sinensis* (31) and *T. vulgaris* (19).

3.2. Molecular docking

The relative stabilities of the complexes constituted of ligands and proteins target were evaluated using docking score assessments, binding affinities, and further molecular dynamics. Table **2** summarizes the estimated binding energies of the 100 ligands docked into the binding site of 6lu7 and 6m0j proteins. According to this docking screening, the most promising results are observed with eighteen compounds.

Table 2: *In silico* binding energies (kcal/mol) of phytoconstituents towards SARS-CoV-2 Mpro (PDB ID: 6lu7) and SP (PDB ID: 6m0j) using docking studies.

Citrus sinensis			*Thymus vulgaris*			*Cymbopogo ncitratus*			*Allium cepa*			*Zingiber officinale*					
N°	6lu7	6m0j	N°	6lu7	6m0j	N°	6lu7	6m0j	N°	6lu7	6m0j	N°	6lu7	6m0j	N°	6lu7	6m0j
01	-5.7	-5.5	17	-8.7	-6.4	32	-7.2	-6.8	51	-4.6	-5.1	67	-8.5	-6.3	83	-6.6	-7.0
02	-5.1	-5.4	18	-8.6	-6.5	33	-7.2	-6.8	52	-4.5	-4.9	68	-9.1	-6.5	84	-7.1	-6.8
03	-5.1	-4.7	19	-4.6	-5.1	34	-7.0	-6.1	53	-4.5	-5.4	69	-8.8	-6.3	85	-6.7	-7.0
04	-6.3	-6.8	20	-4.6	-4.9	35	-5.3	-5.7	54	-4.3	-5.0	70	-4.9	-5.5	86	-6.7	-6.8
05	-6.5	-6.0	21	-4.0	-5.2	36	-4.6	-5.2	55	-4.8	-5.2	71	-5.4	-5.3	87	-5.4	-5.7
06	-5.4	-4.7	22	-4.4	-5.2	37	-4.9	-5.1	56	-4.7	-5.0	72	-5.6	-5.5	88	-5.7	-5.9
07	-5.8	-5.1	23	-4.3	-5.0	38	-4.5	-5.2	57	-4.8	-4.9	73	-5.6	-4.6	89	-6.0	-6.1
08	-7.0	-6.6	24	-4.5	-5.5	39	-4.7	-5.2	58	-4.4	-5.3	74	-8.2	-6.7	90	-6.0	-5.9
09	-8.4	-6.7	25	-5.2	-4.9	40	-4.8	-5.4	59	-4.1	-4.7	75	-7.9	-6.6	91	-7.1	-6.8
10	-8.3	-6.1	26	-4.8	-4.9	41	-4.3	-5.1	60	-4.6	-5.2	76	-5.4	-4.7	92	-6.9	-6.4
11	-8.7	-6.5	27	-5.2	-4.5	42	-5.3	-5.6	61	-8.4	-6.5	77	-7.2	-6.9	93	-6.6	-6.3
12	-8.3	-5.8	28	-4.9	-4.3	43	-7.2	-7.5	62	-4.7	-5.1	78	-7.6	-7.0	94	-6.9	-5.8
13	-8.2	-5.8	39	-4.5	-4.3	44	-6.7	-7.6	63	-4.7	-5.7	79	-8.0	-6.9	95	-6.1	-5.7
14	-7.5	-6.8	30	-4.1	-5.1	45	-7.4	-6.9	64	-4.6	-5.1	80	-7.4	-7.3	96	-7.7	-6.9
15	-8.2	-6.9	31	-3.7	-4.2	46	-8.2	-7.2	65	-5.6	-6.5	81	-7.5	-6.7	97	-6.4	-6.5
16	-8.1	-7.5				47	-8.5	-7.3	66	-4.2	-5.5	82	-8.2	-6.8	*Allium sativum L.*		
						48	-8.6	-7.4							98	-3.6	-3.8
						49	-8.6	-7.0							99	-3.4	-3.6
						50	-7.5	-6.5							100	-3.2	-3.5

Among the ligands suggested to molecular docking, the most promising results are those organized in Table 3, containing eighteen phytoconstituents that can directly bind at two selected target sites: 6lu7 SARS-CoV-2 Mpro and 6m0j SARS-CoV-2 SP. The best score comprises between -8.1 and -9.1 kcal/mol was observed with Mpro. All these molecules could have good inhibitory potential with the studied proteins. Accordingly, they were then inspected for their interactions with the hot spot residues.

Table 3: Summary of 18 top ranked *p*hytoconstituents organized in ascending order of docking scores (BE: binding energy) screened against SARS-CoV-2 Mpro.

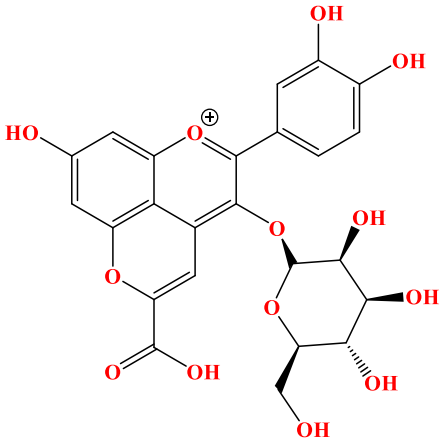

68

3-O-β-glucopyranoside of 5-carboxypyranocyanidin (BE= -9.1)
Plant: *Allium cepa*

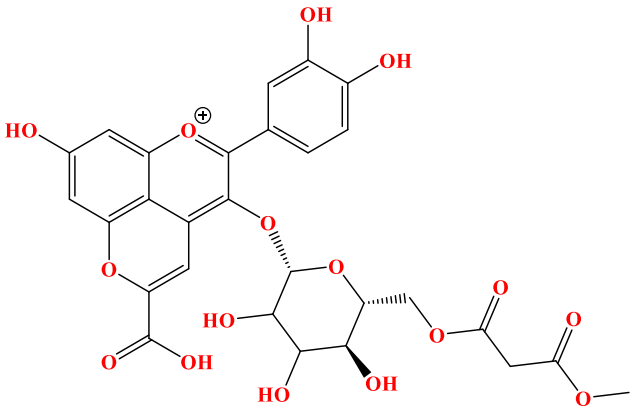

69

5-carboxypyranocyanidin 3-O-(6''-O-methylmalonyl-bglucopyranoside (BE= -8.8)
Plant: *Allium cepa*

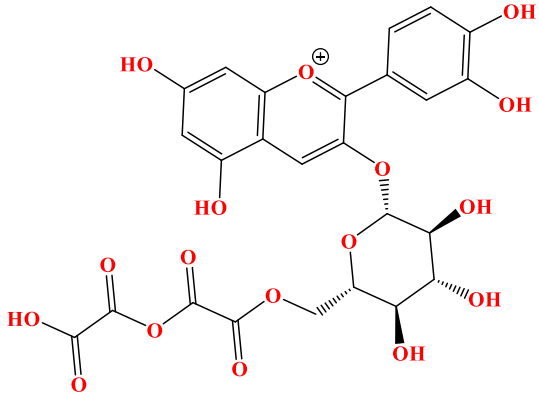

10

Cyanidin 3-O-(6''-dioxalylglucoside) (BE= -8.7)
Plant: *Citrus sinensis*

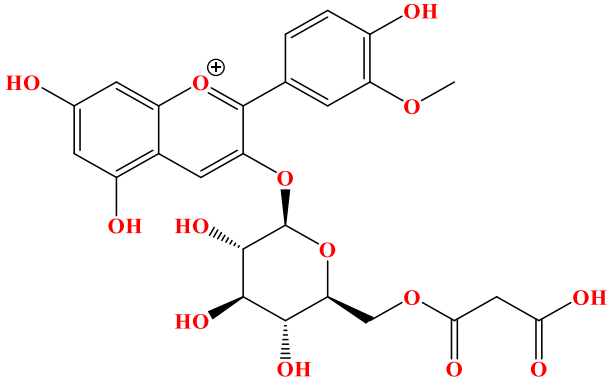

17

Peonidin 3-(6''-malonylglucoside) (BE= -8.7)
Plant: *Citrus sinensis*

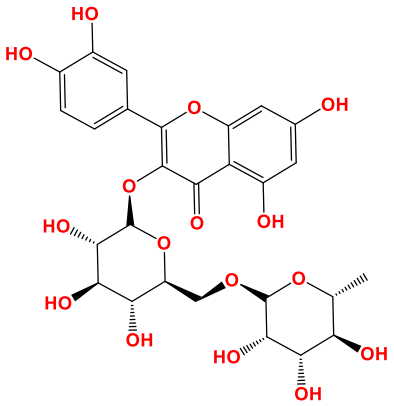

18

Rutin (BE= -8.6)
Plant: *Citrus sinensis*

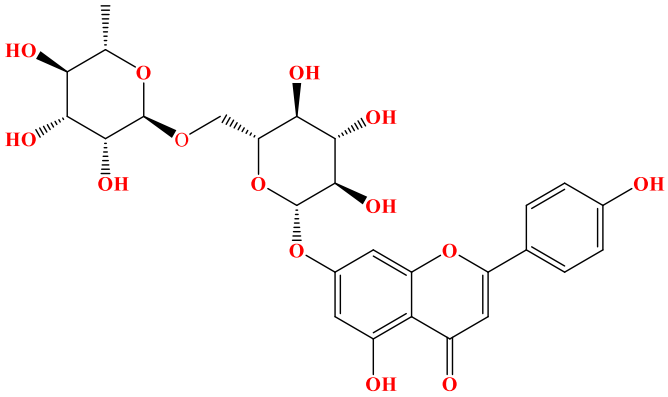

49

Apigenin-7-rutinoside (BE= -8.6)
Plant: *Thymus vulgaris*

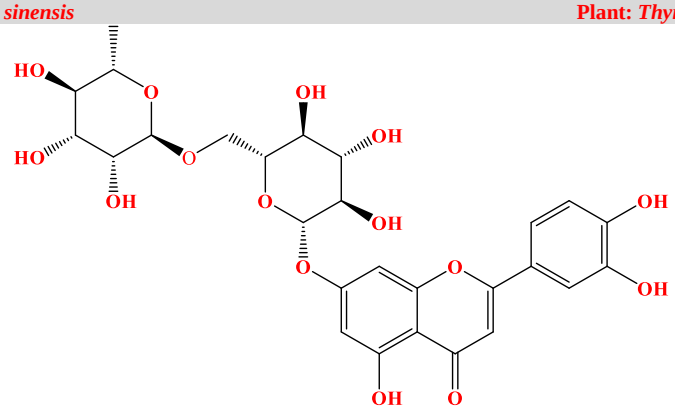

48

Eriodictyol-7-rutinoside (BE= -8.6)
Plant: *Thymus vulgaris*

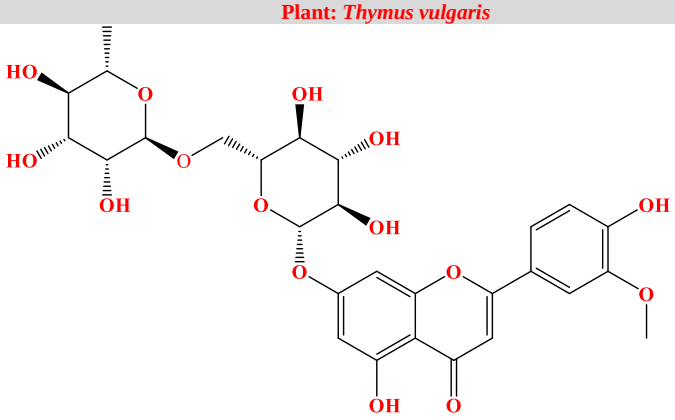

47

Hesperidin (BE= -8.5)
Plant: *Thymus vulgaris*

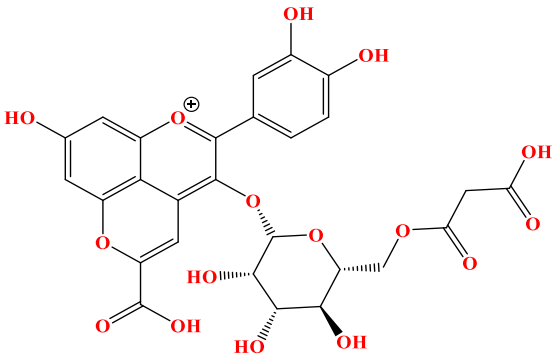

67

3-O-(6''-O-malonyl-β-glucopyranoside) of 5-carboxypyranocyanidin (BE= -8.5)
Plant: *Allium cepa*

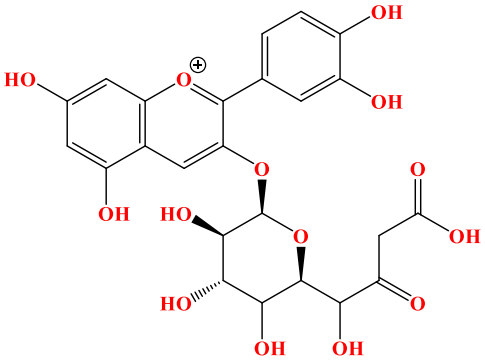

09

Cyanidin 3-(6''-malonylglucoside) (BE= -8.4)
Plant: *Citrus sinensis*

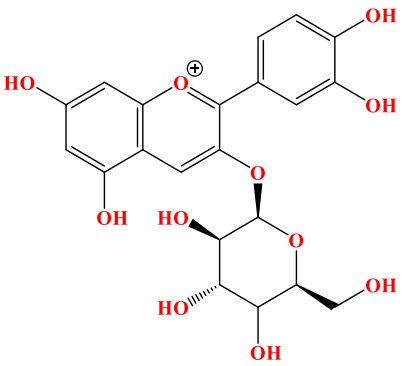

10

Cyanidin 3-glucoside (BE= -8.3)
Plant: *Citrus sinensis*

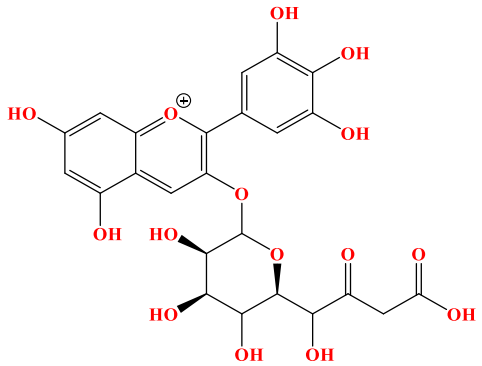

12

Delphinidin 3-(6''-malonylglucoside) (BE= -8.3)
Plant: *Citrus sinensis*

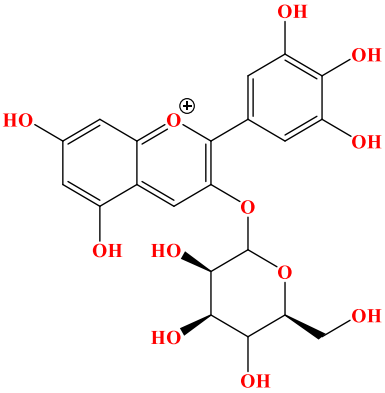

13

Delphinidin 3-glucoside (BE= -8.2)
Plant: *Citrus sinensis*

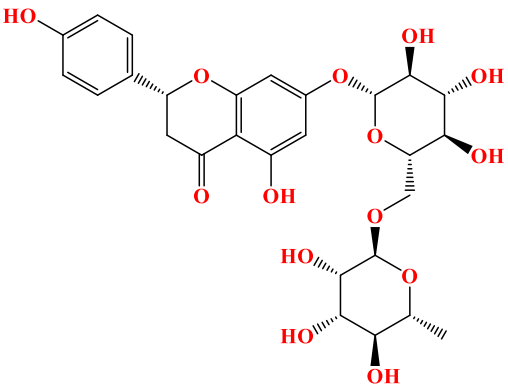

15

Naringin (BE= -8.2)
Plant: *Citrus sinensis*

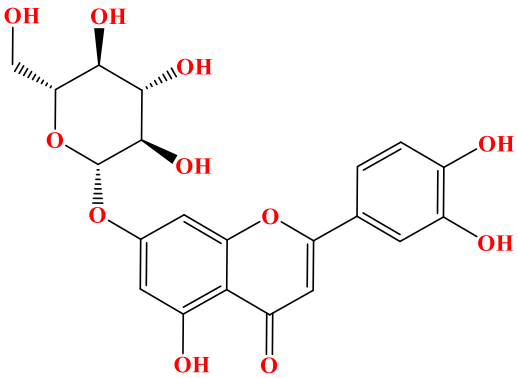

46

Luteolin-7-O-β-glucopyrnoside (BE= -8.2)
Plant: *Thymus vulgaris*

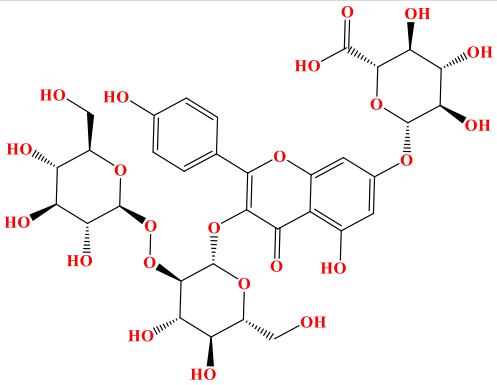

74

Kaempferol 3-O-sophoroside-7-O-glucuronide (BE= -8.2)
Plant: *Allium cepa*

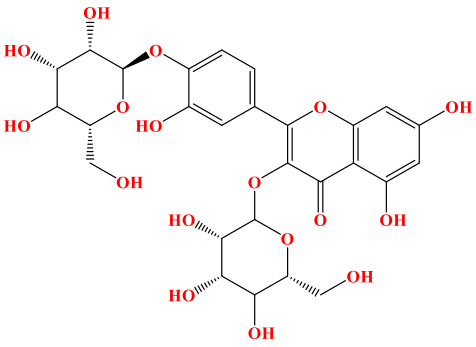

82

Quercetin-3,4'-O-glucoside (BE= -8.2)
Plant: *Allium cepa*

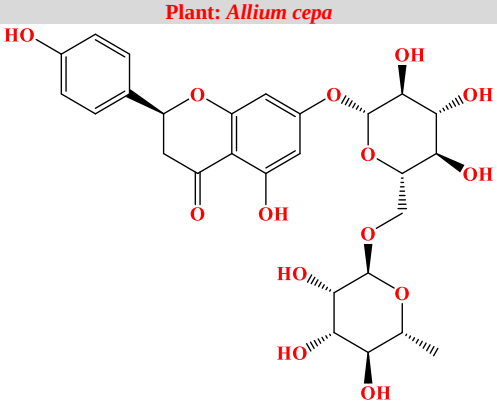

16

Narirutin (BE= -8.1)
Plant: *Citrus sinensis*

3.3. Molecular docking interactions

The molecular docking analysis has been performed to highlight the interaction modes between studied ligands and the targeted proteins. Hence, it seems that the studied ligands interact with targets through three binding modes: hydrogen bonds, interactions between π systems and cation-π interactions, and hydrophobic contacts and non-specific Van der Waals interactions between aliphatic or aromatic carbon atoms.

Discovery Studio visualizer was used to show different binding modes. Fig. 1 and 2 show the binding site of targeted proteins that share interactions with ligands and having a significant energetic contribution to the total energy of interaction.

3.3.1. *SARS-CoV-2 Mpro (PDB ID: 6lu7)*

The high affinity of **10** with 6lu7 is associated with the presence of one conventional hydrogen bond interaction with Met165 at distance 2.90 Å, two carbon hydrogen bonds with Gly143 at 3.05 Å and with Phe160 at 3.57 Å which create a strong cohesive environment, thereby stabilizing the complex formed. There are three hydrophobic π-alky interactions with two Met49 at distances 4.39 and 5.08 Å, and with Cys145 at distance 5.42 Å, also responsible of the conformational stability of **10** (Fig. **1A**). Based on binding affinity, **10** (-8.3 kcal/mol) was among all the studied compounds nominated as the top-ranked compound with a securely bind to the pocket of Mpro through multiple strong covalent and hydrogen bond interactions.

His41 (3.98 Å) was involved in ionic interaction with oxygen at position 1 of Peonidin 3-(6"-malonylglucoside). Compound **17** is stabilized in the binding site of SARS-CoV-2 Mpro 6lu7 by three conventional hydrogen bond interaction with His163, Gly166 and Tyr54 at distances 2.08, 2.19, and 2.53 Å, respectively. The conformational energy of this compound is minimized by the presence of three other π-alkyl interactions with Met49, Met49 and Met145 at distances 4.33, 4.89 Å and 3.45 Å. The presence of π-sulfuric bond with Cys145 (4.97 Å) is also a factor of stabilizing the complex formed (Fig. 1B).

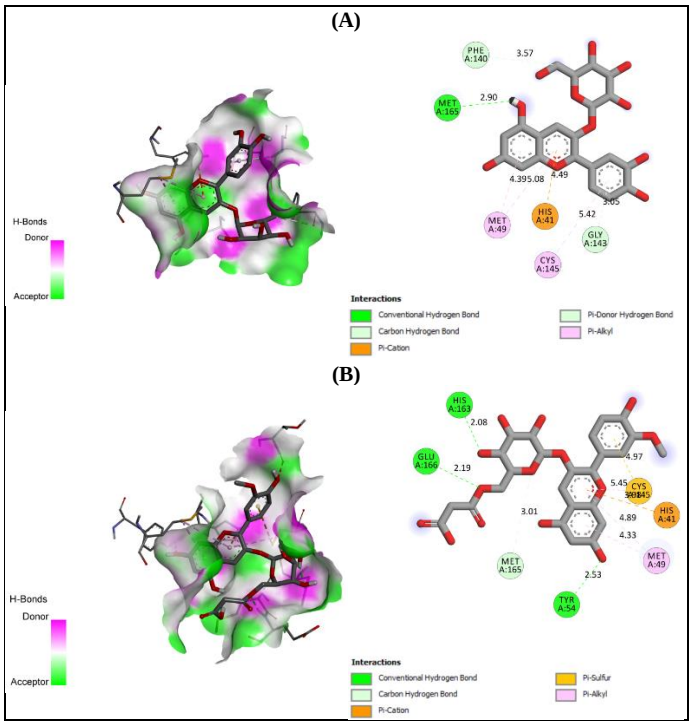

Fig. 1: 2D and 3D interactions and key residues for the inhibitor binding between 6lu7 and (A): Cyanidin 3-glucoside (**10**) (*Citrus sinensis*) and (B): Peonidin 3-(6"-malonylglucoside) (**17**) (*Citrus sinensis*)

3.3.2. SARS-CoV-2 Spike protein (PDB ID: 6m0j)

The conformational energy of the compound 17 is minimized by the presence of four hydrophobic interactions (Pi-alkyl interactions): one with Leu368 and two with Leu335 at the respective distances 5.05, 5.48 and 5.40 Å. These interactions, are mainly associated with the transfer of charge, that help in the intercalation of the drug at the binding site of the enzyme known as (6lu7). The fourth Pi-sigma interaction with Val367 (3.77 Å) amino acid is also beneficial for the stability of this conformation (Fig. 2A).

The conformational energy of the ligand is also minimized by three other Pi-alkyl interactions (hydrophobic interactions). One Pi-alkyl interaction with Val367 located at distance 5.07 Å, and two Leu335 and Leu368 amino acids, which are located at distances of 5.04, and 5.09 Å. These interactions, involving charge transfer, help in the intercalation of the ligand at the binding site of the enzyme. The conformational energy of **17** is also minimized by the presence of two conventional hydrogen bonds, with the following amino acids: Ser371 (2.53 Å) and Phe338 (2.86 Å). There are also two additional carbon hydrogen bonds with Gly339 amino acid at distances 3.67 Å and 3.68 Å (Fig. 2B).

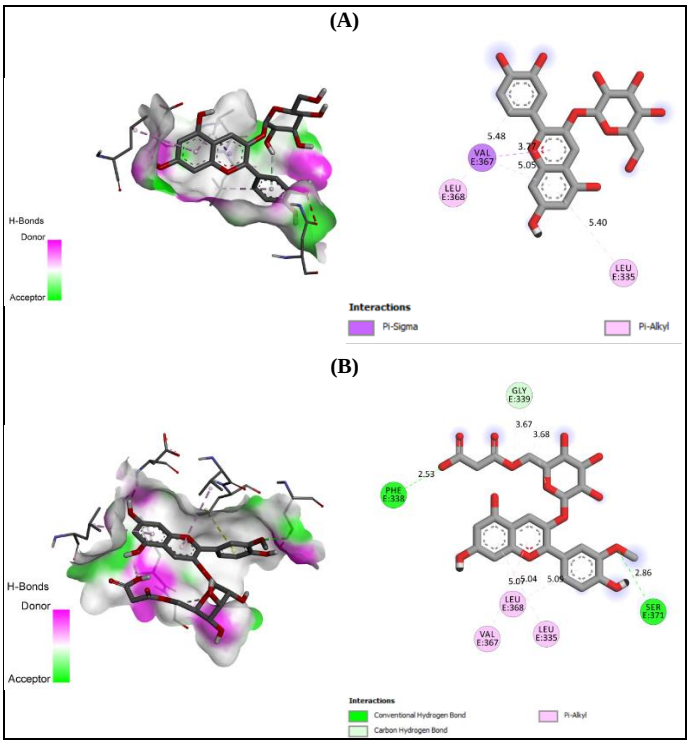

Fig. 2: 2D and 3D interactions and key residues for the inhibitor binding between 6m0j and (A): Cyanidin 3-glucoside (**10**) (*Citrus sinensis*) and (B): Peonidin 3-(6"-malonylglucoside) (**17**) (*Citrus sinensis*)

3.4. Pharmacokinetic processes

Predicting the absorption, distribution, metabolism, excretion and toxicity (ADMET) parameters in drug development is an important step to prevent drug failure in clinical stages. The ADMET results are presented in tables **4** to **7**.

Prediction of absorption process

Absorption is the process by which the unchanged drug passes from its site of administration into the general circulation. Oral medications for must essentially cross at least one cell membrane to act. Several parameters can be check to validate the absorption process, one of which is solubility. It is one of the major descriptors, the decimal logarithm of the molar solubility in water in log S (mol/l) appear in table 5. We can see that all compounds have good solubility in the water (Insoluble ≤ -10 < poorly soluble < -6 < Moderately < -4 < soluble < -2 < very soluble < 0 ≤ highly soluble). Beside the solubility, can be added the Caco-2 permeability.

Caco-2 permeability, intestinal absorption (human), and skin permeability, were also used to predict the absorption level of the potential hit compounds.

During the last twenty years, the human intestinal Caco-2 cell line has been widely served as a model to in vitro simulate the physical and biochemical barrier of the human intestine. Caco-2 cells are a kind of epithelial cell line that has become a standard in pharmaceutical drug transport studies [45].

They express hundreds of transporters [46], and they have high prediction capacity of the fraction of oral dose absorbed in humans [47], although being far from ideal [48]. The absorption of orally delivered medicines and other xenobiotics is routinely predicted using permeability coefficients across monolayers of the human Caco-2 cell line grown on permeable supports. All of the screened compounds showed a weak predicted Caco-2 permeability ranged from 0.85 to -0.9 cm/s (log Papp values < 0.90 cm/s), as shown in table 5.

Concerning skin permeability (log Kp<-2.5), all compounds are considered to show a relatively high skin permeability.

In fact, molecules with predicted intestinal absorption values less than 30% are considered poorly absorbed. Prediction of human intestinal absorption is a major goal in the development of oral drugs since absorption influences bioavailability and the response intensity. Table 4 showed a poorly predicted intestinal absorption of fifteen compounds among the eighteen screened. However, compounds **10** (38 %), **17** (31%) and **46** (37%) showed moderated absorption.

Table 4: Prediction of absorption for the top ranked phytoconstituents against SARS-CoV-2 Mpro

Compounds	Water solubility log S (mol/l)	Caco2 permeability log Papp (cm/s)	Intestinal absorption (%)	Skin permeability log Kp
09	-2.892	-0.973	0	-2.735
10	-3.191	-0.807	37.774	-2.735
11	-2.900	-0.848	6.37	-2.735
12	-2.892	-0.956	0	-2.735
13	-2.972	-0.861	28.766	-2.735
15	-2.584	-0.588	20.414	-2.735
16	-2.584	-0.588	20.414	-2.735
17	-3.06	0.189	31.142	-2.735
18	-2.909	-0.354	24.758	-2.735
46	-3.228	0.169	36.734	-2.735
47	-2.939	-0.095	26.758	-2.735
48	-2.935	-0.097	22.049	-2.735
49	-2.908	-0.167	24.972	-2.735
67	-2.190	0.850	0	-2.735
68	-2.988	-0.343	29.003	-2.735
69	-2.977	0.688	20.411	-2.735
74	-2.892	-0.779	0	-2.735
82	-2.886	-0.540	0	-2.735

Prediction of distribution process

When a drug enters the systemic circulation, it generally spreads throughout the body. Volume of distribution at steady-state (VDss), blood-brain barrier (BBB) and central nervous system (CNS) permeability are some parameters that can be investigated *in silico* with considerable accuracy in order to define the transport of chemicals throughout different compartments within the body.

According to Table 5, potential hit compounds have low values of Log BB and Log PS (log BB<-1 and log PS<-3) and have showed overall, low permeability at the level of the BBB and CNS. As already mentioned by Fan and Lannoy [36] and observed in this work, compound that is highly plasma protein bound will generally exhibit a small volume of distribution, whereas one that is extensively bound to tissue components will exhibit a VDss that can be much greater than the physiological volume of the body. The values of VDss of the compounds ranged from -0.679 to 0.410 cm/s. Compounds **11**, **18**, **46**, **47**, **48**, **49**, **68**, **74** and **82** showed a VDss< 0, suggesting their strong binding to plasma proteins, which is not favorable and **46** (VDss= -0.032) has most caught our attention, hence its exclusion from the list of the greatest potential candidates. On the other hand, the volumes of distribution of the others nine compounds (**9**, **10**, **12**, **13**, **15**, **16**, **17**, **67** and **69**) are >0, indicating their distribution in the extracellular water.

Prediction of excretion process

Generally, the irreversible removal of a compound or its metabolite(s) from the body is referred to as excretion, which is mainly facilitated by renal or biliary clearance. Clearance is the body's overall ability to eliminate a molecule, defined as the volume of completely cleansed plasma per unit of time; it is commonly given as a flow rate in ml/min. Estimating clearance is essential for evaluating the compound's efficacy, duration of action, and concentration in the body, as well as avoiding harmful effects. Organs such as the kidneys, liver, lungs, and others can remove substances from the body. As a result, total body clearance equals to the sum of the substance's clearance by each organ.

The human organic cation transporter 2 (OCT2) is a multi-specific organic cation transporter that transports a variety of clinically used drugs. OCT2 is a key transporter in the active secretion of organic cations in the kidney and is primarily responsible for the absorption of organic cations across the basolateral membrane of renal tubular epithelial cells [49].

Excretion profile of the compounds was predicted as showed in table 5 using Cation transporter 2 (OCT2) and drug total clearance parameter (CLtot).

According to the results of the prediction of the total clearance for compounds **10, 11, 13, 17, 46**, and **68** are the highest compared to other compounds. Low values of total clearance for **10, 11, 13, 17, 46** and **68** illustrate high half-life for these compounds while negative values **9**, **12**, **15**, **16**, **18**, **47**, **48**, **49**, **67**, **69**, **74** and **82** illustrate low half-life and plausible stumpy toxic effect.

The results also suggest that the screened compounds may not be substrates for organic cation transporter 2 (OCT2), which is important for the excretion of cationic molecules and suggested the absence of systemic overexposure or cytotoxicity by intracellular accumulation linked to the consumption of these compounds. From the result above, we can considerate that the compounds excreted through kidney in another mechanism besides OCT2.

Table 5: Prediction of distribution and execration proprieties for the top ranked phytoconstituents against SARS-CoV-2 Mpro

Compounds	Distribution			Execration	
	VDss	BBB permeability Log BB	CNS permeability Log PS	Total Clearance CLtot	Renal OCT2 substrate
9	0.410	-2.309	-5.297	-0.663	No
10	0.097	-1.763	-4.964	0.797	No
11	-0.468	-2.681	-5.419	1.110	No
12	0.053	-2.603	-5.687	-0.838	No
13	0.041	-2.084	-4.832	0.782	No
15	0.182	-1.669	-4.797	0.434	No
16	0.182	-1.669	-4.797	0.434	No
17	0.189	-2.273	-4.989	0.941	No
18	-0.340	-1.991	-5.890	0.032	No
46	-0.032	-1.650	-4.480	0.737	No
47	-0.413	-1.820	-5.228	0.127	No
48	-0.190	-1.820	-5.238	0.061	No
49	-0.244	-1.643	-4.929	0.207	No
67	0.055	-2.211	-5.284	0.003	No
68	-0.679	-2.206	-5.232	0.988	No
69	0.048	-2.208	-5.211	0.060	No
74	-0.152	-2.842	-7.692	0.137	No
82	-0.455	-2.252	-6.128	-0.043	No

Prediction of metabolism process

The study of an active substance's metabolism is mostly a descriptive approach to the numerous metabolic pathways and their relative importance, as well as the effects on the drug's activity and disposal. The term metabolism refers to the transformation of a drug into one or more pharmacologically active or inactive compounds via an enzymatic process. The liver contains the majority of these drug-metabolizing enzymes, although they can also be found in other tissues, in particular the lungs. The metabolism of pharmaceuticals and other foreign chemicals (xenobiotics) involves three types of biotransformation reactions: oxidation-reduction, hydrolysis, and conjugation [50]. A high number of enzymes involved in drug processing are found in hepatocytes.

Cytochrome P450, which is made up of several isoenzymes, is the primary building block of this enzymatic system.

Cytochrome P450 (CYP) enzymes are hemeproteins that play a key role in drug metabolism; as a result, investigating metabolic inactivation and/or activation may prevent failure in clinical studies and can allow medicinal chemists to introduce new functional groups on the molecule to avoid the metabolic pathways that can lead toxic or very polar compounds that can be easily eliminated from the body. Furthermore, this can aid in the development of metabolically stable drugs, as well as avoiding drug-drug interactions. We believe that these molecules are promising inhibitors for Mpro and SP of SARS-CoV-2 based on their observed safety. All of the screened compounds screened were neither substrates nor selective inhibitors for the subtypes of cytochrome P450 family of enzymes, as shown in table 6. This suggests that all of the compounds might be metabolized directly in the liver, without interfering with the metabolism of another drug. Hence, potential side effects from drug biotransformation after administration of these compounds are unlikely.

Table 6: Prediction of metabolism for the top ranked phytoconstituents against SARS-CoV-2 Mpro

Compounds	Cyp1A2	Cyp2C19	Cyp2D6	Cyp3A4
09	No	No	No	No
10	No	No	No	No
11	No	No	No	No
12	No	No	No	No
13	No	No	No	No
15	No	No	No	No
16	No	No	No	No
17	No	No	No	No
18	No	No	No	No
46	No	No	No	No
47	No	No	No	No
48	No	No	No	No
49	No	No	No	No
67	No	No	No	No
68	No	No	No	No
69	No	No	No	No
74	No	No	No	No
82	No	No	No	No

Prediction of toxicological properties

The toxicity of a substance can be defined as the degree that substance is poisonous or can cause injury. It depends on a variety of factors: dose, duration and route of exposure, shape and structure of the chemical itself, and individual human factors. The typical toxicology profile consists of safety pharmacology, genetic toxicology, acute and subchronic toxicology, absorption, distribution, metabolism, and excretion (ADME) studies, reproductive and developmental toxicity, and an evaluation of carcinogenic potential [51].

From the results of toxicological predictions in table **7**, it appears AMES toxicity for five compounds (**13**, **18**, **46**, **48** and **49**). Moreover, regarding the hepatotoxicity, the results are as follows; all compounds tested are predicted to have no toxic risk to liver function, may not inhibit the hERG channel, and may not have skin sensitization.

This indicates that the lead compounds could not cause mutation in DNA of the test organism and therefore may not act as carcinogen. A repeated exposure to these compounds could not be able to provoke adverse health effect of dermatitis. This result is of paramount importance since; skin sensitization is the endpoint aiming at the identification of chemicals able to elicit an allergic response in susceptible individuals. Since hepatotoxicity is an adverse reaction that can be rare but serious and caused by drugs, Table **7** shows that exposure to these potential drugs should not be the cause of injury or damage to the liver.

Table 7 shows that the LD50 values of the selected compounds were found to be greater than 2.314 mol/kg, indicating that the compounds are only fatal at extremely large doses.

Table 7: Toxicological prediction of the selected compounds

Compounds	Ames toxicity	Herg1 inhibition	LD50 (mol/Kg)	Hepatotoxicity	Skin sensitisation
09	No	No	2.569	No	No
10	No	No	2.858	No	No
11	No	No	2.567	No	No
12	No	No	2.502	No	No
13	Yes	No	2.702	No	No
15	No	No	2.933	No	No
16	No	No	2.933	No	No
17	No	No	2.727	No	No
18	Yes	No	2.329	No	No
46	Yes	No	2.432	No	No
47	No	No	2.354	No	No
48	Yes	No	2.314	No	No
49	Yes	No	2.520	No	No
67	No	No	2.459	No	No
68	No	No	2.539	No	No
69	No	No	2.737	No	No
74	No	No	2.478	No	No
82	No	No	2.323	No	No

ADMET investigations revealed that Cyanidin 3-glucoside (**10**) and Peonidin 3-(6"-malonylglucoside) (**17**) have excellent predicted absorption, distribution, metabolism and toxicity properties, implying that they could be developed as orally-active lead molecules. As a result, these compounds were chosen as model for MD to investigate their stability at the binding sites of the Mpro (PDB ID: 6lu7) and SP (PDB ID: 6m0j) proteins.

3.5. Molecular Dynamic simulation

The dynamics of the M pro and SP proteins, as well as their complexes (lead compounds 10 and 17), were tracked and analyzed using a physiological environment similar to protein models in aqueous systems. The molecular conformations with the lowest binding energy towards the targeted Mpro and SP proteins were used as templates in the current MD simulation experiment to properly evaluate their structural stability in the studied systems (Ligand-protein).

Analysis of RMSD and RMSF

The initial analysis MD simulation results was performed by calculating the RMSD of backbone of all structures with respect to their respective initial structures. The RMSD of all systems is shown in **Fig. 3A**. As evident from the data, all systems reached equilibrium in first few initial nanoseconds of simulation then remain sable throughout the simulation period. The average RMSD of Mpro, Mpro-compound 10 complex and Mpro-compound **17** complex were found to be 0.29, 0.19, and 0.22 nm, respectively. Similar result was obtained for SP and their complexes. The average RMSD of complexes of SP were slightly higher than SP alone but still within the acceptable range. Moreover, the visual analysis of the trajectories clearly showed the systems reached equilibrium and providing preliminary evidence regarding the stability of systems under physiological conditions. Further analysis of the systems was carried out by calculating their RMSF. The RMSF of C_α atoms of each residue of both proteins and complexes is shown in **Fig. 3B**.

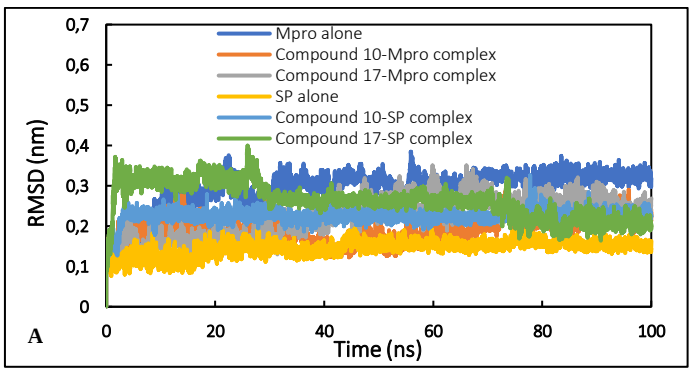

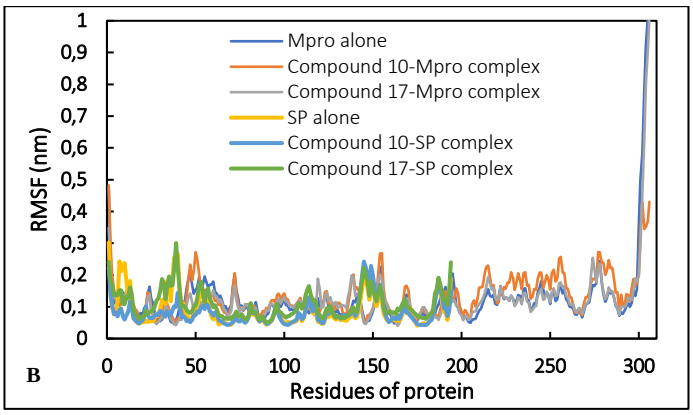

Fig. 3. (A) Root mean square deviation (RMSD) of uncomplexed Mpro and SP and complexed with compounds **10** and **17**. (B) Root mean square fluctuation (RMSD) Cα atoms of uncomplexed Mpro and SP and complexed with compounds **10** and **17**.

The RMSF of most of the residues of both proteins in absence and presence of compounds **10** and **17** was found to be below 0.2 nm, indicating a good stability of the amino acids under aqueous environment. Few residues, especially terminal ones, showed more fluctuations, which is owed their hanging position, and tend to fluctuate. Moreover, the RMSF pattern of complexes of both proteins were similar to their proteins alone counter parts. This shows that the complexes are equally stable in physiological environment. The dynamic nature of ligands was assessed by calculating the RMSF of each atom of ligands. The RMSF of ligands is presented in **Fig. 4**. Certain atoms all ligands showed some fluctuation indicating the dynamical their shift at their binding site.

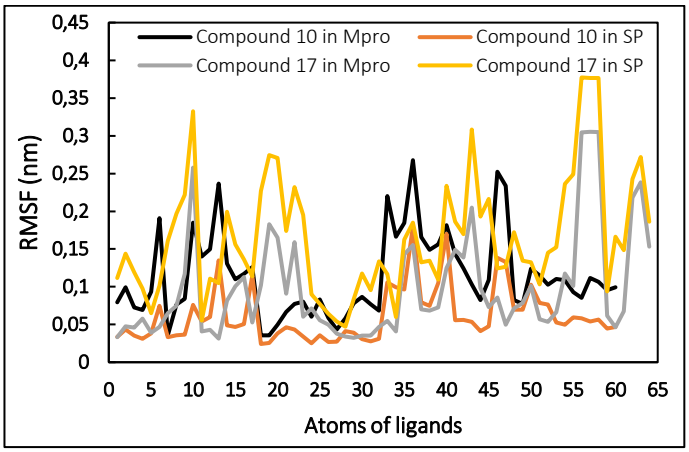

Fig. 4. RMSF individual atoms of compounds **10** and **17** in complexed with Mpro and SP.

Assessment of Rg and SASA, and energies

Radius of gyration (R_g) is defined as the mass-weighted RMS distance of collection of atoms from their common center of mass. R_g is considered an important parameter for studying the stability of protein in MD simulations [52]. In globular and compact proteins, there are less variations in R_g compared to the proteins of expanded form structures [5]. The R_g of Mpro and SP in the absence and presence of compounds **10** and **17** are shown in **Fig. 5A**. The data clearly shows that there was negligible fluctuation in R_g over simulation time. For instance, the average R_g of Mpro, Mpro-compound **10** complex and Mpro-compound **17** complex were found to be 2.18, 2.20 and 2.20 nm, respectively. A similar result was obtained for SP and its complexes. These values show that both proteins and their complexes were quite stable in the aqueous systems. Furthermore, the analysis of R_g also showed that both the proteins did not undergo major conformational changes in presence of ligands [53]. Solvent accessible surface area (SASA) is another important parameter to study the stability of proteins and their complexes in MD simulations. The SASA of Mpro and SP and their complexes are presented in **Fig. 5B**. As evident from the data, there was negligible fluctuation in SASA of all systems over the simulation time. For example, the average SASA of Mpro, Mpro-compound **10** complex and Mpro-compound **17** complex were found to be 150.29, 145.38, and 146.90 nm^2, respectively. A similar result was SP and its complexes. The data further validates the stability of all systems under physiological environment.

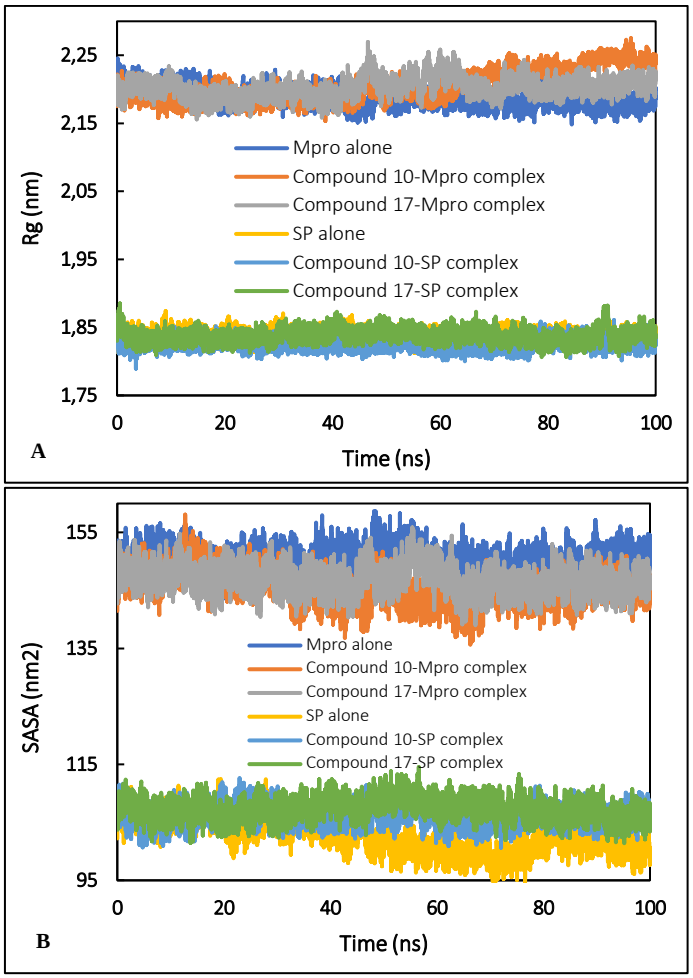

Fig. 5. (A) Radius of gyration (Rg) of uncomplexed Mpro and SP and complexed with compounds **10** and **17** as a function of time. (B) Solvent accessible surface area (SASA) of uncomplexed Mpro and SP and complexed with compounds **10** and **17** as a function of time.

Additionally, the physicochemical parameters such as total energy and potential energy of the systems were also calculated (**Fig. 6**). The energies of all systems were found to be constant over entire simulation period again validating stabile nature of all systems through MD simulation.

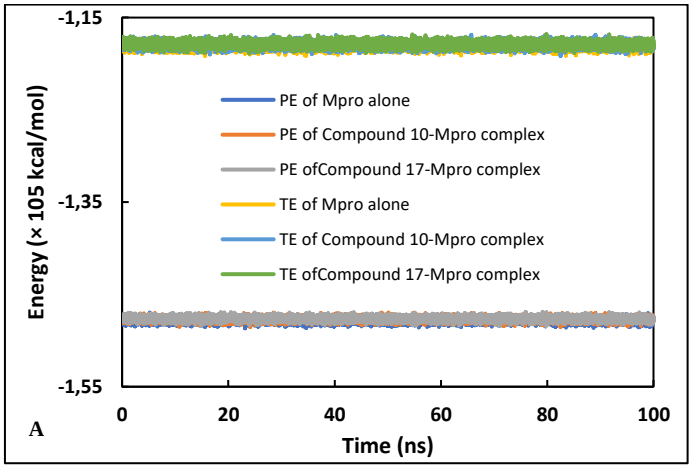

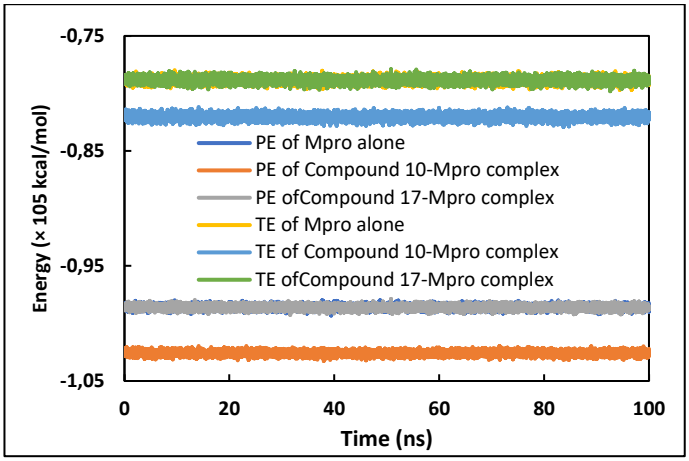

Fig 6. (A) The potential energy and total energy of uncomplexed Mpro and complexed with compounds **10** and **17** as a function of time. (B) The potential energy and total energy of uncomplexed SP and complexed with compounds **10** and **17** as a function of time.

Assessment of the structural stability and hydrogen bonds

The effect of interaction of compounds **10** and **17** in the structural stability of Mpro and SP was explored by calculating their secondary structures. The average secondary structural motifs of Mpro and SP in absence and presence of ligands is shown in **Fig. 7**. There were negotiable effects of the secondary structure components of both proteins in the presence of compounds **10** and **17**. For instance, the average percentage of coil, β-sheet, β-bridge, bend, turn, and α-helix was found to be 25.59, 25.59, 2.08, 8.43, 16.88, and 16.70, respectively. All these secondary structural motifs were negligibly altered in presence of compounds **10** and **17**. Similarly, there was negligible changes in secondary structure of SP in the presence of both ligands. The data confirm that the presence of compounds **10** and **17** affected the structural stability of Mpro and SP.

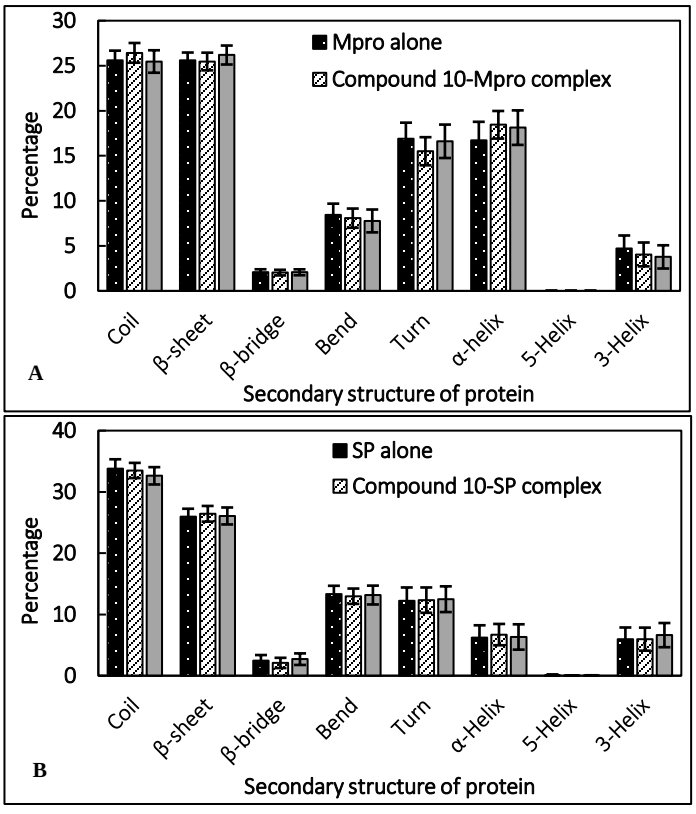

Fig. 7. (A) Percentage of secondary structure in uncomplexed Mpro and complexed with compounds **10** and **17**. (A) Percentage of secondary structure in uncomplexed SP and complexed with compounds **10** and **17**.

The interaction of compounds **10** and **17** with Mpro and SP was studied by computing the hydrogen bond profiles. As evident from the hydrogen bond profiles, there existence of hydrogen bonds between ligands and proteins throughout the simulation period. The number of hydrogens bonds as function of time is presented in **Fig. 8**. The average number of hydrogen bonds formed by compounds **10** and **17** with Mpro was obtained as 1.37 and 1.43, respectively. There was lesser number of hydrogen bonds formed by the ligands with SP. In all complexes, we note the existence of hydrogens bonds throughout the entire simulation period. However, there were some variations in hydrogen bond profiles which is due to dynamical shift of the ligands within the binding site.

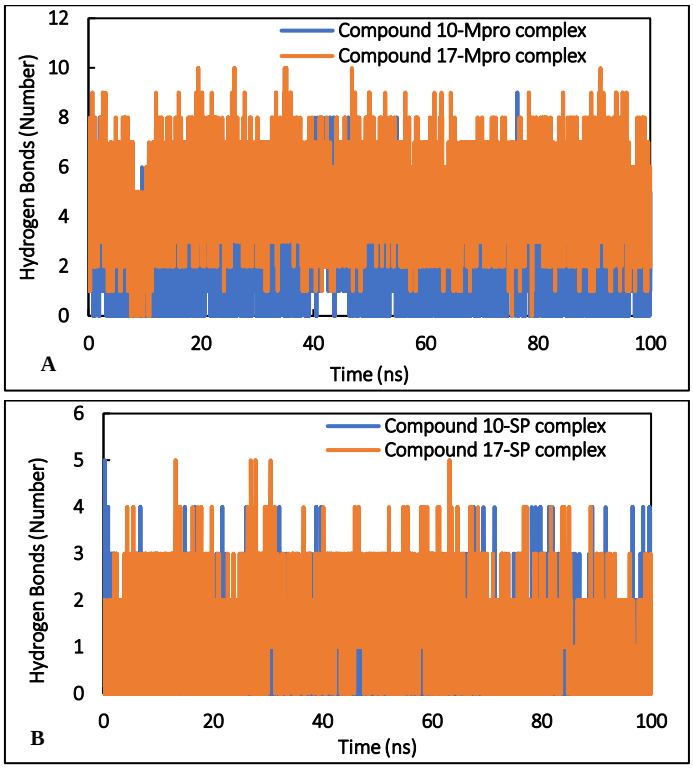

Fig. 8. (A) Number of hydrogen bonds of formed by compounds **10** and **17** with Mpro as function of time. (B) Number of hydrogen bonds of formed by compounds **10** and **17** with SP as function of time.

Principal component analysis

Principal component analysis (PCA) is a standard statistical procedure to analyse the large-scale motion in biological macromolecules such as proteins and DNA. PCA is performed by reducing the dimensionality of data set without losing important information, which is characterized by eigenvectors [54]. PCA was performed to explore the relative flexibility in both in the presence and absence of compounds **10** and **17**. The projection of eigenvectors SP and Mpro in the absence and presence of ligands is presented in **Fig. 9**.

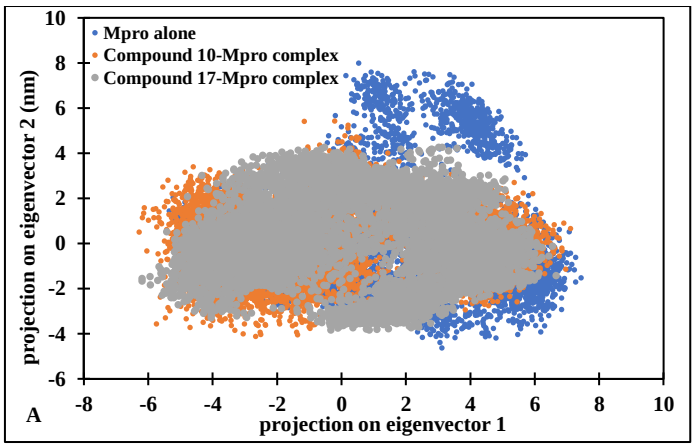

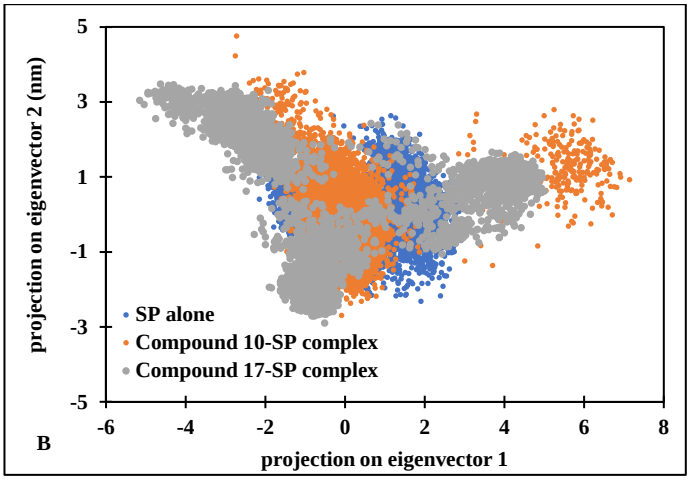

Fig. 9. (A) Principal component analysis (PCA) of uncomplexed Mpro and complexed with compounds **10** and **17**. Principal component analysis (PCA) of uncomplexed SP and complexed with compounds **10** and **17**.

The projection shows that Mpro-compound **10** complex and Mpro-compound **17** complex occupied a similar conformational space. Mpro complexes alone occupied slightly different conformational space. However, the total conformational space occupied by Mpro alone its complexes was roughly same. This indicates that the complexation of both ligands to Mpro did not alter the structural flexibility of the protein. On contrary, both the complexes of SP exhibited more conformational space than SP alone, showing the binding of ligands increased the overall structural flexibility of SP.

Additionally, free energy landscapes (FEL) of the proteins and their complexes were plotted to analyses the pattern of protein folding (**Fig. 10**). The FEL plots show that all systems reached their energy minima in the landscapes. The structure exhibiting lowest energy were extracted and then Ramachandran plots of these energy minima structures were made. The Ramachandran plots of Mpro and SP in the absence and presence of compound **10** and compound **17** showed that almost all amino acids were found the favorable region, again showing their stability.

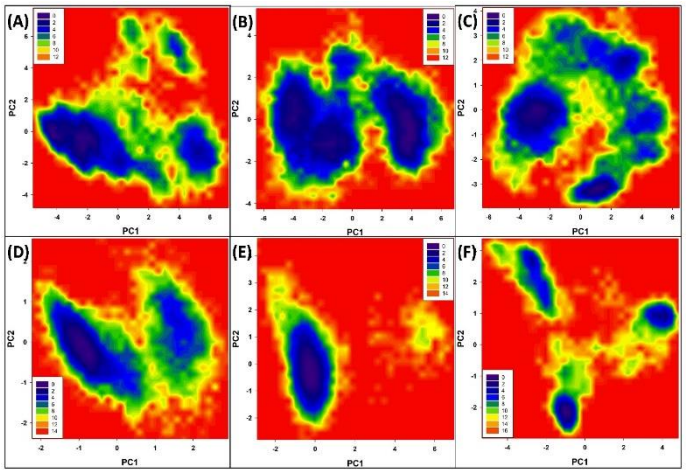

Fig. 10. (A) Free energy landscape plot of Mpro alone. (B) Free energy landscape plot of Mpro-compound **10** complex. (C) Free energy landscape plot of Mpro-compound **17** complex. (D) Free energy landscape plot of SP alone. (E) Free energy landscape plot of SP-compound **10** complex. (F) Free energy landscape plot of SP-compound **17** complex.

MM-PBSA calculation

MM-PBSA calculations were used to investigate the nature of various binding energies involved in the binding of Mpro and SP with both ligands. For the MM-PBSA calculations, 100 frames from each complex's trajectory were extracted. Non- covalent forces are usually prominent in protein-ligand interactions. Hydrogen bonds, electrostatic forces, Van Der Waals forces, hydrophobic interactions, and other forces are examples. Each of these forces contributes to the overall binding energy in either a positive or negative way [55]. **Table 8** lists the MM-PBSA binding energies for the interactions of compounds **10** and **17** with Mpro and *S* proteins. The interaction of compound 10 with Mpro was greatly favored by Van der Waals energy, SASA and electrostatic energy played a little role as well. The binding of compound **17** to Mpro was supported by electrostatic and Van Der Waals energies. The Van Der Waals energy was the most important factor in the interaction of both ligands with *S* protein. In addition, SASA and electrostatic energy played a minor role in this interaction. The binding of both ligands to both proteins was hampered by polar solvation energy. Compounds **10** and **17** had binding energies of -20.85 and -64.26 kcal mol^{-1}, respectively, when they interacted with Mpro. Binding energies for **10** and **17** with *S* protein were also found to be -28.84 and -11.20 kcal mol^{-1}, respectively.

Table 8. Binding free energy (kcal mol^{-1}) for the interaction of compounds **10** and **17** with Mpro and SP using MMBSA analysis.

Type of energy	Mpro		SP	
	Compound 10	Compound 17	Compound 10	Compound 17
ΔE_{vdW}	-39.08±0.56	-55.40±0.35	-43.92±0.28	-32.78±0.38
ΔE_{ele}	-7.87±0.29	-55.79±0.38	-3.60±0.19	-1.46±0.52
ΔE_{PSE}	30.19±0.70	51.74±0.36	22.88±0.19	26.48±0.58
ΔES_{SASA}	-4.08±0.03	-4.80±0.02	-4.19±0.01	-3.42±0.03
ΔE_{BE}	-20.85±0.41	-64.26±0.44	-28.84±0.28	-11.20±0.38

ΔE_{vdW}: van der Waal energy, ΔE_{ele}: Electrostatic energy, ΔE_{PSE}: Polar solvation energy, ΔE_{SASA}: Solvent accessible surface area energy, ΔE_{BE}: Binding energy.

The MM-PBSA analysis was further used for identification of the key residues exhibiting maximum contribution in the overall binding energy. The major energy contributing residues is enlisted (Tables **9** and **10**). The major energy contributing residues for interaction of compound **10** with Mpro were Thr-25 Leu27, Met49, Met165, Asp187, and Gln189. Similarly, Glu14, Glu47, Asp48, Glu55, Asp56, Glu166, Asp176, Glu178, Asp187, Asp197, Asp289, and Glu290 were the key energy contributors for compound **17**-Mpro interaction.

The major contributing residues for compound **10**-SP interaction were obtained as Phe338, Gly339, Phe342, Val367, Leu368, Phe374, Ile434, and Trp436. The key energy contributors in compound **17**-SP interaction were Glu340, Asp364, Asp389, Asp398, Asp442, Glu516, and Gly526.

Table 9. The average polar, apolar and total binding energies (kcal mol^{-1}) of the key residues of Mpro.

Residues	Compound 10				Compound 17		
	E_{polar}	E_{Apolar}	E_{total}	Residues	E_{polar}	E_{Apolar}	E_{total}
Thr-25	0.174	-0.087	-0.538	Glu-14	0.296	0	-3.034
Leu-27	0.251	-0.014	-0.630	Glu-47	0.551	0	-4.758
Met-49	0.171	-0.047	-0.555	Asp-48	1.734	0	-4.552
Met-165	1.004	-0.170	-1.510	Glu-55	0.553	0	-3.847
Asp-187	0.657	-0.035	-0.668	Asp-56	0.442	0	-3.549
Gln-189	2.863	-0.296	-0.706	Glu-166	9.170	-0.273	-4.166
				Asp-176	1.212	0	-3.535
				Glu-178	0.441	0	-3.143
				Asp-187	5.708	-0.053	-6.213
				Asp-197	0.386	0	-3.340
				Asp-289	0.230	0	-3.000
				Glu-290	0.289	0	-3.239

E_{polar}: Polar energy; E_{Apolar}: Apolar energy; E_{total}: Total energy.

Table 10. The average polar, apolar and total binding energies (kcal mol^{-1}) of the key residues of SP.

Residues	Compound 10				Compound 17		
	E_{polar}	E_{Apolar}	E_{total}	Residues	E_{polar}	E_{Apolar}	E_{total}
Phe-338	0.383	-0.092	-0.720	Glu-340	1.417	-0.002	-5.419
Gly-339	0.199	-0.129	-0.871	Asp-364	4.236	-0.038	-5.249
Phe-342	1.684	-0.262	-3.185	Asp-389	0.166	0.000	-3.266
Val-367	0.541	-0.329	-2.577	Asp-398	0.903	0	-3.612
Leu-368	0.135	-0.081	-1.653	Asp-442	0.775	0.000	-4.289
Phe-374	0.277	-0.047	-1.069	Glu-516	0.273	0.000	-3.009
Ile-434	0.068	-0.016	-0.815	Gly-526	0.456	-0.00	-3.939
Trp-436	0.847	-0.109	-1.682				

E_{polar}: Polar energy; E_{Apolar}: Apolar energy; E_{total}: Total energy.

CONCLUSION

Since 2019, COVID-19 has been the major outbreak in almost all the nations worldwide. Our recent drug repurposing studies proposed few phytoconstituents that target SARS-CoV-2 Mpro and SP proteins and suggested that they could be used as target in COVID-19 off setting. Therefore, it is essential to remain investigate other plants in order to discover potential compounds that may inhibit SARS-CoV-2 proliferation without sides effects and serve as potential anti-COVID-19 drugs. We now, developed a library from approved apiphytotherapy that contains numerous natural compounds, and screened them against the SARS-CoV-2 Mpro and SP. The Mpro, whit score comprises between -8.1 and -9.1 Kcal/mol turned out to be the best target for potential hits compounds.

The interaction analysis reveals that amino acids Met49, Met169, Phe 160, Phe 338, Gly143, Gly339, His41, His163, Cys145, Tyr54, Ser371, Leu335, Leu368 and Val367 could have important role in the formation of complexes. Based on the prediction of different pharmacokinetic parameters, we have found ten compounds exhibiting satisfactory ADME characteristics because they have good solubility, high VDss, are no inhibitors for the cytochrome P450 family enzymes, appreciated total clearance, and may not be substrates for OCT2, which is important for the excretion of cationic molecules. Our analyses identified two non-toxic (Cyanidin 3-glucoside and Peonidin 3-(6"-malonylglucoside) obtained from *Citrus sinensis*), leads compounds that are predicted to bind with two receptors binding site of SARS-CoV-2. They can be investigated for chemical transformations and further for *in vitro* revisions for drug discovery to fight Sars-CoV-2. Moreover, *Citrus sinensis* that is widely consumed in Cameroon would once again be a source to be explored in the fight against Covid-19 pandemic.

AUTHOR CONTRIBUTION: RTF AND HPDF

Data curation, Writing, Original draft preparation; SB and MB: Visualization, Validation; MO and FAQ: Conceptualization, Writing, Original draft preparation. SC: Writing, Original draft preparation, Conceptualization, Methodology, Software, Supervision.

- Romuald Tematio Fouedjou, Hervet Paulain Dongmo Fogang, Ossama Daoui and Monisa Ayoub : Data curation, Writing, Original draft preparation;

- Farhan Siddique, Souad Elkhattabi and Mohamed Bakhouch : Visualization, Validation;

- Samir CHTITA: Writing, Original draft preparation, Conceptualization, Methodology, Software, Supervision.

FUNDING

We would like to express our gratefulness to the "Agence Universitaire de la Francophonie (AUF)" for funding this research project (reference: AUF-DRM6588. Title: *Composé dérivés de l'eugénol : hémisynthèse ciblée via la relation structure activité et investigation de l'activité anti-SARS-CoV-2*).

CONFLICTS OF INTEREST

There are no conflicts to declare.

DATA AVAILABILITY STATEMENT

All data used in this work are private.

CODE AVAILABILITY STATEMENT

The codes used in this work are not available.

REFERENCES

1. WHO, Geneva, Switzerland, Coronavirus disease 2019 (COVID-19) Situation Report, 38, (2020).
2. H. Lu, Drug treatment options for the 2019-new coronavirus (2019-nCoV), *Biosci Trends*, 16, **14**, 1, 69-71, (2020).
3. T. Pillaiyar, S. Meenakshisundaram, M. Manickam, Recent discovery and development of inhibitors targeting coronaviruses, *Drug Discovery Today*, **25**, 4, 668-688, (2020).
4. O. Daoui, S. Elkhattabi, S. Chtita, Rational identification of small molecules derived from 9,10-dihydrophenanthrene as potential inhibitors of 3CLpro enzyme for COVID-19 therapy: a computer-aided drug design approach, Struct. Chem. (2022). https://doi.org/10.1007/s11224-022-02004-z.
5. T. R. Fouedjou, S. Chtita, M. Bakhouch, S. Belaidi, M. Ouassaf, A. L. Djoumbissie, A. L. Tapondjou, A. F. Qais, Cameroonian Medicinal plants as Potential candidates of SARS-CoV-2 Inhibit, *J. Biomol. Struct. Dyn*, (2021).
6. A. Sofowora, Plantes médicinales et médecine traditionnelle d'Afrique, Paris, Ed Karthala, 375, (1996).
7. J. Tchoumboué, I. R. Tchouamo, J. Y. Pinta, M. N. Njia, Caractéristiques socioéconomiques et techniques de l'apiculture dans les Hautes Terres de l'Ouest du Cameroun, *Tropicultura*, **19**, 3, 141-146, (2001).
8. K. P. R. Fotso, F. Meutchieye, S. I. Andriamanalina, A. Youbissi, J. Tchoumboué, J. Y. Pinta, P. Zango, Caractéristiques socio-économiques et techniques de l'apiculture dans les Départements de Bamboutos, Mifi et Menoua (Région de l'Ouest-Cameroun). Livestock Research for Rural Development. 26, 221, (2014).
9. R. D. Nnomo, I. R. Tchouamo, J. Y. Pinta, Apiphytothérapie à base du miel au Cameroun, *Ethnopharmacologia*, 44, 56-63, (2009).
10. M. Chirilă, E. Neguţ, A. Herold, P. Chirilă, G. Szegli, The epurox therapy in allergic bronchic asthma and chronic obstructive bronchitis--clinical insights, Arch. Roum. Pathol. Exp. Microbiol., 46(3):267-75, (1987).
11. S. Chtita, A. Belhassan, A. Aouidate, S. Belaidi, M. Bouachrine, T. Lakhlifi, Discovery of potent SARS-CoV-2 inhibitors from approved antiviral drugs via docking and virtual screening, Comb. Chem. High Throughput Screening, **24**, 3, 441-454, (2021).
12. Dassault Systèmes, BIOVIA, Discovery Studio Visualizer, San Diego: Dassault Systèmes BIOVIA (2020). Available from: http://www.3dsbiovia.com/products/collaborative-science/biovia-discovery-studio/visualization-download.php
13. D. Schoeman, C. B. Fielding, Coronavirus envelope protein: current knowledge. *Virol. J.*, **16**, 69, 1-22, (2019).
14. R. R. Narkhede, S. R. Cheke, J. P. Ambhore, S. D. Shinde, The Molecular Docking Study of Potential Drug CandidatesShowing Anti-COVID-19 Activity by Exploring of TherapeuticTargets of SARS-CoV-2. *Eurasian J. Med and Oncol*, **4**, 3, 185-195, (2020).
15. F. Li, W. Li, M. Farzan, S. C. Harrison, Structure of SARS corona virus spike receptor-binding domain complexed with receptor. *Sci*, 309, **5742**, 1864-1868, (2005).
16. F. Li, Structure, Function, and Evolution of Coronavirus Spike Proteins. *Annu Rev Virol*, **3**, 237-61, (2016).
17. H. Kikuzaki, S. M. Tsai, N. Nakatanit, Gingerdiol Related Compounds from the rhizomes of *Zingiber officinale*. *Phytochemistry* **31**, 5, 1783-1786, (1992).
18. J. J. Araya, H. Zhang, T. E. Prisinzano, L. A. Mitscher, B. N. Timmermann, Identification of unprecedented purine-containing compounds, the zingerines, from ginger rhizomes (*Zingiber officinale* Roscoe) using a phase-trafficking approach. *Phytochemistry*, 72, 935-941, (2011).
19. S. W. Lee, J. H. Lim, S. M. Kim, J. H. Jeong, G. Y. Song, S. W. Lee, C. M. Rho, Phenolic compounds isolated from *Zingiber officinale* roots inhibit cell adhesion. *Food Chem*, **128**, 3, 778-782, (2011).
20. J. J. Mahanta, M. Chutia, M. Bordoloi, M. G. Pathak, R. K. Adhikary, T. C. Sarma, *Cymbopogon citratus* L. essential oil as a potential antifungal agent against key weed moulds of *Pleurotus* spp. Spawns. *Flavour Fragrance J*., 22, 525-530, (2007).

21. I. H. N. Bassoléa, A. Lamien-Meda, B. Bayala, L. C. Obame, A. J. Ilboudo, C. Franz, J. Novak, R. C. Nebié, M. H. Dicko, Chemical composition and antimicrobial activity of *Cymbopogon citratus* and *Cymbopogon giganteus* essential oils alone and in combination. *Phytomedicine* 18, 1070-1074, (2011).
22. J. C. Sepúlveda-Arias,L. A. Veloza, L. M. Escobar, Orozco, I. A. Lopera, Anti-inflammatory effects of the main constituents and epoxides derived from the essential oils obtained from *Tagetes lucida*, *Cymbopogon citratus*, *Lippia alba* and *Eucalyptus citriodora*. *Journal Essent Oil Res*, 1-8, (2013).
23. D. Prakash, N. B. Singh, G. Upadhyay, Antioxidant and free radical scavenging activities of phenols from onion (*Allium cepa*). *Food Chem* 102, 1389-1393, (2007).
24. M. L. Mogren, E. M. Olsson, E. U. Gertsson, Quercetin content in stored onions (*Allium cepa* L.): effects of storage conditions, cultivar, lifting time and nitrogen fertiliser level, *J. Sci. Food Agric.*, 87, 1598-1602, (2007).
25. M. I. Vagen, R. Slimestad. Amount of characteristic compounds in 15 cultivars of onion (*Allium cepa* L.) in controlled field trials, *J. Sci. Food Agric*., 88, 404-411, (2008).
26. L., Ji, F. T. Yuan, G. A. Wang, B. J. Yang, L. Y. Su, Two new furostanol saponins from the seeds of *Allium cepa* L., Chin. *Chem. Lett.*, 19, 461-464, (2007).
27. H. X. Wang, & T. B. Ng. Isolation of Allicepin, a Novel Antifungal Peptide from Onion (*Allium cepa*) Bulbs, *J. Pept. Sci.* , 10, 173-177, (2004)
28. R. Li, W. C. Chen, W. P. Wang, W. Y. Wen-yan Tian, X. G. Zhang, Extraction of essential oils from garlic (*Allium sativum*) using ligarine as solvent and its immunity activity in gastric cancer rat. *Med. Chem Res*, 19, 1092-110, (2010).
29. S. B. Mitiku, M. Sawamura, T. Itoh, H. Ukeda, Volatile components of peel cold-pressed oils of two cultivars of sweet orange (*Citrus sinensis* (L.) Osbeck) from Ethiopia. *Flavour Fragrance J.*, 15, 240-244, (2000).
30. S. Selli, H. Kelebek, Aromatic profile and odour-activity value of blood orange juices obtained from Moro and Sanguinello (*Citrus sinensis* L. Osbeck), *Ind. Crops Prod*, 33, 727-733, (2001).
31. H. Kelebek, H. Canbas, S. Selli, Determination of phenolic composition and antioxidant capacity of blood orange juices obtained from cvs. Moro and Sanguinello (*Citrus sinensis* (L.) Osbeck) grown in Turkey, *Food Chem*, 107, 1710-1716, (2008).
32. M. Hudaib, T. Aburja, Volatile components of *Thymus vulgaris* L. from wild-growing and cultivated plants in Jordan, *Flavour Fragrance J.*, 22, 322-327, (2007).
33. C. M. M. Coelho, C. de M. Bellato, J. C. P. Santos, E. M. M. Ortega, S. M. Tsai, Effect of phytate and storage conditions on the development of the "hard-to-cook". *J. Sci. Food. Agric*., 1243, 1237-1243, (2007).
34. M. Hudaib, E. Speroni, A. M. Di Pietra, V. Cavrini, GC/MS evaluation of thyme (*Thymus vulgaris* L.) oil composition and variations during the vegetative cycle, *J. Pharm. Biomed. Anal.*, 29, 4, 691-700, (2002).
35. M. C Rota, A. Herrera, R. M. Martínez, J. A. Sotomayor, M. J. Jordán, Antimicrobial activity and chemical composition of *Thymus vulgaris*, *Thymus zygis* and *Thymus hyemalis* essential oils. *Food Control*, **19**, 7, 681-687, (2008).
36. J. Fan, I. A. M. de Lannoy, Pharmacokinetics, *Rev. Biochem Pharmacol*, 87, 93-120, (2014).
37. D. E. V Pires,T. L. Blundell, D. B. Ascher, pkCSM: Predicting small-molecule pharmacokinetic and toxicity properties using graph-based signatures, *J Med Chem.* **58**, 9, 4066-4072, (2015).
38. D. Van Der Spoel, E. Lindahl, B. Hess, G. Groenhof, A. E. Mark, H. J. C. Berendsen, GROMACS: Fast, flexible, and free, *J. Comput. Chem.*, **26**, 16, 1701–1718, (2005).
39. J. A. Maier, C. Martinez, K. Kasavajhala, L. Wickstrom, K. E. Hauser, C. Simmerling, ff14SB: Improving the Accuracy of Protein Side Chain and Backbone Parameters from ff99SB, J. Chem. *Theory Comput.*, **11**, 8, 3696–3713, (2015).
40. A. W. Sousa Da Silva, W. F. Vranken, ACPYPE - AnteChamber PYthon Parser interfacE. BMC Research Notes, (2012).
41. G. Bussi, D. Donadio, M. Parrinello, Canonical sampling through velocity rescaling, *J. Chem. Phys*, **126**, 1, 014101, (2007).
42. M. Parrinello, A. Rahman, Polymorphic transitions in single crystals: A new molecular dynamics method, *J. Appl. Phys.*, **52**, 12, 7182–7190, (1981).
43. R. Kumari, R. Kumar, A. Lynn, g_mmpbsa —A GROMACS Tool for High-Throughput MM-PBSA Calculations, *J. Chem. Inf. Model.*, **54**, 7, 1951–1962, (2014).
44. C. A. Lipinski, F. Lombardo, B. W. Dominy, P. J. Feeney, Experimental and computational approaches to estimate solubility and permeability in drug discovery and development settings, Adv. *Drug Delivery Rev.*, 1(46), 3-26, (2001).
45. C. Awortwe, S. P Fasinu, B. Rosenkranz, Awortwe C, Fasinu PS, Rosenkranz B. Application of Caco-2 cell line in herb-drug interaction studies: current approaches and challenges. *J. Pharm. Pharm. Sci.*, 17, 1-19, (2014).
46. T. Hayashi, C. Xu, R. W. Carthew. Cell-type-specific transcription of prospero is controlled by combinatorial signaling in the Drosophila eye. Development 135(16), 2787-2796, (2008).
47. C. Hilgendorf, G. Ahlin, A. Seithel, P. Artursson, A. L. Ungell, J. Karlsson, Expression of thirty-six drug transporter genes in human intestine, liver, kidney, and organotypic Cell Lines. *Drug Metab. Dispos.*, 35, 8, 1333-1340, (2007).
48. A. M. Marino, M. Yarde, H. Patel, S. Chong, P. V. Balimane, Validation of the 96 well Caco-2 cell culture model for high throughput permeability assessment of discovery compounds, *Int. J. Pharm.*, 297, 1-2, 235-241, (2005).
49. T. Fujita, J. T Urban, K. M. Leabman, K. Fujita, M. K. Giacomini, Transport of drugs in the kidney by the human organic cation transporter, OCT2 and its genetic variants, *J. Pharm. Sci.*, **95**, 1, 25-36, (2006).
50. M. S. Alavijeh, M. Chishty, M. Z. Qaiser, A. M. Palmer, Drug metabolism and pharmacokinetics, the blood-brain barrier, and central nervous system drug discovery. *J. Arm. Soc. Exp. NeuroTher.*, 4, 554-571, (2005).
51. M. A. Dorato, L. A. Buckley, Toxicology testing in drug discovery and development, current protocols in toxicology, (2007).
52. F. A. Qais, T. Sarwar, I. Ahmad, R. A. Khan, S. A. Shahzad, F. M. Husain, Glyburide inhibits non-enzymatic glycation of HSA: An approach for the management of AGEs associated diabetic complications, *Int. J. Biol. Macromol*., 169, 143-152, (2021).
53. B. Rath, F. Abul Qais, R. Patro, S. Mohapatra, T. Sharma, Design, synthesis and molecular modeling studies of novel mesalamine linked coumarin for treatment of inflammatory bowel disease, *Bioorg. Med. Chem. Lett*., 128029, (2021).
54. S. Siddiqui, F. Ameen, T. Kausar, S. M. Nayeem, S. Ur Rehman, M. Tabish, Biophysical insight into the binding mechanism of doxofylline to bovine serum albumin: An *in vitro* and *in silico* approach, *Spectrochim. Acta, Part A*, 249, 119296, (2021).
55. S. Siddiqui, F. Ameen, I. Jahan, S. M. Nayeem, M. Tabish, A comprehensive spectroscopic and computational investigation on the binding of the anti-asthmatic drug triamcinolone with serum albumin, *New J. Chem*., **43**, 10, 4137-4151, (2019).